catalysts

MDPI

Article

Pd–Au Bimetallic Catalysts for the Hydrogenation of Muconic Acid to Bio-Adipic Acid

Sofia Capelli [1], Ilaria Barlocco [1], Federico Maria Scesa [1], Xiaohui Huang [2], Di Wang [2], Francesca Tessore [1], Alberto Villa [1], Alessandro Di Michele [3] and Carlo Pirola [1,*]

[1] Chemistry Department, Università degli Studi di Milano, Via Golgi 19, 20133 Milan, Italy; sofia.capelli@unimi.it (S.C.); ilaria.barlocco@unimi.it (I.B.); federicomaria.scesa@studenti.unimi.it (F.M.S.); francesca.tessore@unimi.it (F.T.); alberto.villa@unimi.it (A.V.)

[2] Institute of Nanotechnology, Karlsruhe Institute of Technology, Hermann-von-Helmholtz-Platz 1, 76344, Eggenstein-Leopoldshafen, Germany; xiaohui.huang@partner.kit.edu (X.H.); di.wang@kit.edu (D.W.)

[3] Department of Physics and Geologia, University of Perugia, Via Pascoli, 06123 Perugia, Italy; alessandro.dimichele@unipg.it

* Correspondence: carlo.pirola@unimi.it; Tel.: +39-02-5031-4283

Abstract: The hydrogenation reaction of muconic acid, produced from biomass using fermentative processes, to bio-adipic acid is one of the most appealing green emerging chemical process. This reaction can be promoted by catalysts based on a metal belonging to the platinum group, and the use of a second metal can preserve and increase their activity. Pd–Au bimetallic nanoparticle samples supported on high-temperature, heat-treated carbon nanofibers were prepared using the sol immobilization method, changing the Pd–Au molar ratio. These catalysts were characterized by TEM, STEM, and XPS analysis and tested in a batch reactor pressurized with hydrogen, where muconic acid dissolved in water was converted to adipic acid. The synthesized Pd–Au bimetallic catalysts showed higher activity than monometallic Au and Pd material and better stability during the recycling tests. Moreover, the selectivity toward the mono-unsaturated changed by decreasing the Pd/Au molar ratio: the higher the amount of gold, the higher the selectivity toward the intermediates.

Keywords: adipic acid; muconic acid; bimetallic catalysts; palladium; gold; deactivation

Citation: Capelli, S.; Barlocco, I.; Scesa, F.M.; Huang, X.; Wang, D.; Tessore, F.; Villa, A.; Di Michele, A.; Pirola, C. Pd–Au Bimetallic Catalysts for the Hydrogenation of Muconic Acid to Bio-Adipic Acid. *Catalysts* **2021**, *11*, 1313. https://doi.org/10.3390/catal11111313

Academic Editor: Gilles Berhault

Received: 29 September 2021
Accepted: 27 October 2021
Published: 29 October 2021

1. Introduction

The industrial success of emerging biomass conversion processes lies in the correct design and synthesis of a robust heterogeneous catalyst. Often, catalyst deactivation occurs due to metal leaching or poisoning of the active sites. In particular, fouling or metal leaching is observed when a catalyst is prepared by using a metal belonging to the platinum group (platinum group metal (PGM)) [1]. Moreover, the choice of the support plays a key role in catalyst reactivation because normally the regeneration occurs in a strong oxidative environment at high temperature. Therefore, the development of a stable catalyst is the key point to increase the economic feasibility of green industrial processes. Nowadays, researchers are developing a new family of next-generation catalysts for renewable energy and chemicals synthesis having high productivity and durability [2].

The hydrogenation of muconic acid (MA) to bio-adipic acid (AdA) is one of the emerging green chemical processes that deal with PGM catalysts durability challenges. MA is a dicarboxylic acid widely studied for the production of bio-based bulk chemicals (i.e., adipic acid) or bio-privileged molecules, and it can be produced from lignocellulosic biomass using both biological and catalytic processes [3–7]. In the past years, PGM-based catalysts have been widely used for the reduction of MA: Pt and Pd supported on activated carbon have been successfully used to hydrogenate MA [8–12]. However, metal

leaching occurs when performing the reaction in a strong acidic environment [13]. The addition of a second metal tends to preserve and increase catalyst activity, thus enhancing the whole performance of the material and making the process economically more sustainable [14,15]. In fact, metal nanoparticles (NPs) composed of two different metals exhibit unique and peculiar catalytic properties that are different with respect to the monometallic counterpart. In particular, a synergistic effect is created, which generates distinctive and new properties, allowing an increase in the selectivity toward the desired products [16]. The synergistic effect is not yet completely clear; nevertheless, two main hypotheses were formulated to explain this phenomenon. The first one is called the electronic (or ligand) effect, which is defined as a change in metal electronic properties due to heterometallic bonds. The second one is the dilution (or ensemble) effect, which is established when the active metal is diluted in a second metal at an atomic scale [17]. Concerning PGMs, many bimetallic systems can be synthesized using different synthetic techniques (sol immobilization, impregnation, precipitation). In particular, various Pd-based bimetallic catalysts have been successfully synthesized using Ag [18], Rh [19], Cu [20], Pt [21], and Au [22] as a second metal. Pd–Au bimetallic systems have been widely used in hydrogenation reactions, and compared to the monometallic Au and Pd material, the bimetallic samples always show the best performance in terms of conversion, selectivity, and stability [22–27]. Monometallic Pd NPs supported on carbonaceous material were already reported as an active catalyst for the MA hydrogenation reaction, with an activity of about 650 h^{-1} [12]. Despite the good activity, many studies have reported the leaching of the active metal [28,29], and due to the increase in the price of Pd, this behavior should be reduced as much as possible. Therefore, considering the synergistic effect of a bimetallic catalyst for the enhancement in catalyst stability, in this work Pd–Au bimetallic NPs supported on a highly graphitized support (high-temperature, heat-treated carbon nanofibers (HHT CNFs)) were prepared using the sol immobilization method [30]. Commercial HHT CNFs were used as a support for the deposition of different bimetallic Pd–Au NPs prepared by changing the Pd/Au molar ratio.

The positive effect of Au as a second metal in the catalyst formulation was demonstrated for the conversion and selectivity of the reaction. Moreover, the catalyst stability during the recycle test was higher for the bimetallic sample. The Pd/Au molar ratio is a key parameter for the mono-unsaturated product: the higher the amount of gold, the higher the selectivity toward the intermediates.

2. Results and Discussion

2.1. Characterization

The catalysts were characterized by TEM (Transmission Electron Microscopy) and XPS (X-Ray Photoelectron Spectroscopy) analysis. The catalysts' morphology, particle size distribution, and bulk Pd/Au ratio were evaluated by TEM and HAADF-STEM (Scanning Transmission Electron Microscopy) analyses. Monometallic Pd and Au catalysts showed an average particle size of 3.9 ± 1.2 nm and 3.4 ± 1.2 nm, respectively. All the bimetallic catalysts displayed a mean particle dimeter of about 3.0 nm, with a narrow particle size distribution (PSD), except for the Pd_4Au_6 sample, which showed an average particle size of 4.0 ± 0.8 nm (Figures 1–4). By using STEM-XEDS analysis, the amount evaluation of Pd and Au for a single NP was performed. The calculated values are in agreement with the nominal ones, except for the Pd_2Au_8 sample (Table 1). The estimated Pd/Au molar ratio for this catalyst was 0.15, which is lower than the nominal one (0.25). This behavior could be ascribed to the presence of segregated Pd NPs. Moreover, the images suggest the formation of a Pd–Au alloy structure with enrichment of Pd on the NP surface.

Table 1. Results of TEM-EDX analysis.

Catalyst	Pd/Au$_{nominal}$ (molar ratio)	Pd/Au$_{EDX}$ (molar ratio)	Pd/Au$_{nominal}$ (molar ratio)	Pd/Au$_{EDX}$ (molar ratio)	Average particle size (nm)
Pd/HHT	-	-	-	-	3.9 ± 1.2
Pd_8Au_2/HHT	8.0–2.0	8.3–1.7	4.0	4.8	3.5 ± 0.9
Pd_6Au_4/HHT	6.0–4.0	5.9–4.1	1.5	1.4	2.9 ± 0.7
Pd_4Au_6/HHT	4.0–6.0	4.5–5.5	0.67	0.82	4.0 ± 0.8
Pd_2Au_8/HHT	2.0–8.0	1.3–8.7	0.25	0.15	3.1 ± 0.6
Au/HHT	-	-	-	-	3.4 ± 1.2

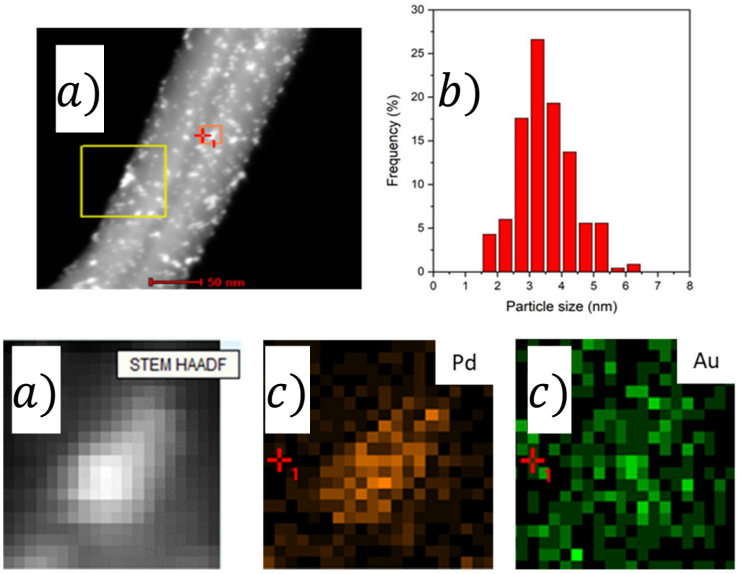

Figure 1. (**a**) TEM, (**b**) NP size distribution, and (**c**) EDX analysis of Pd_8Au_2 catalyst.

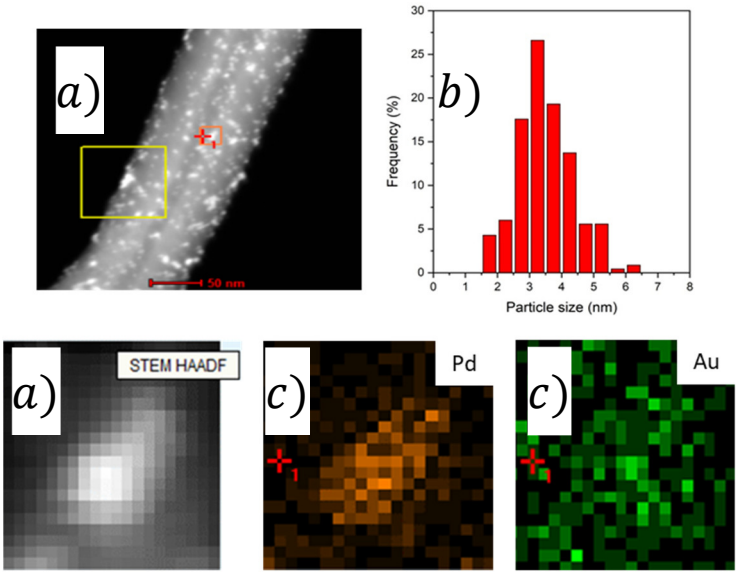

Figure 2. (**a**) TEM, (**b**) NP size distribution, and (**c**) EDX analysis of Pd_6Au_4 catalyst.

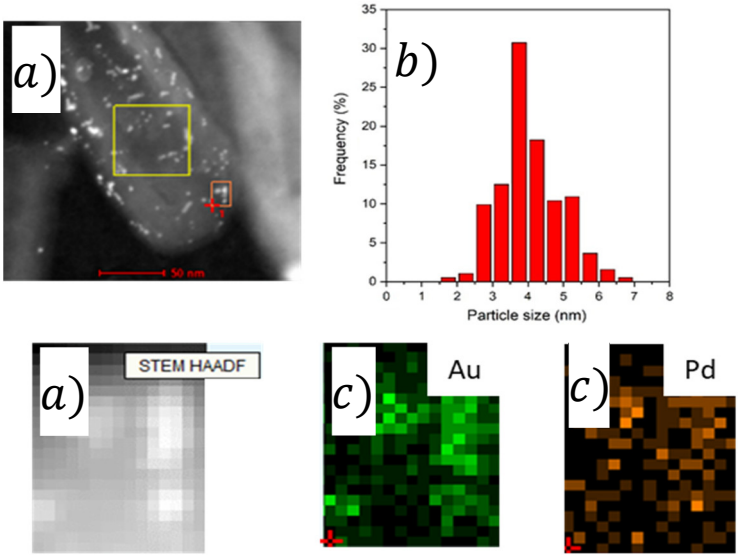

Figure 3. (**a**) TEM, (**b**) NP size distribution, and (**c**) EDX analysis of Pd_4Au_6 catalyst.

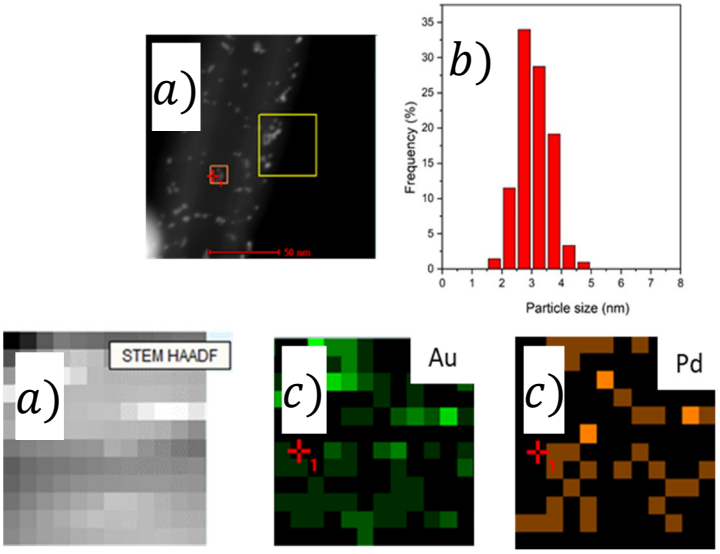

Figure 4. (**a**) TEM, (**b**) NP size distribution, and (**c**) EDX analysis of Pd_2Au_8 catalyst.

XPS analysis was also used to study the surface composition of the oxidation state and relative metals' amount. Four main species were revealed by the survey spectra: gold (Au 4f 83.3–84.2 eV), carbon (C 1s 284.2–284.6 eV), palladium (Pd 3d 335.4–337.6 eV), and oxygen (O 1s 532.2–532.6 eV). Considering the superficial Pd/Au molar ratio ($Pd/Au_{surface}$), lower values than nominal ones were calculated (Table 2). This indicates that the catalyst surface is Pd rich, as also previously observed from STEM-XEDS analyses.

Table 2. Results of XPS survey spectra [30].

Catalyst		C 1s	O 1s	Au 4f	Pd 3d	$Pd/Au_{nominal}$	$Pd/Au_{surface}$
Pd/HHT	B.E. (eV)	284.6	532.6	-	337.6	-	-
	%At.	92.1	7.3	-	0.6		
Pd_8Au_2/HHT	B.E. (eV)	284.2	532.2	83.4	335.4	4.0	6.5
	%At.	91.2	7.3	0.2	1.3		
Pd_6Au_4/HHT	B.E. (eV)	284.4	532.4	83.4	335.4	1.5	1.5
	%At.	95.5	3.5	0.4	0.6		
Pd_4Au_6/HHT	B.E. (eV)	284.3	532.3	84.3	335.6	0.7	1.0
	%At.	96.2	3.1	0.3	0.3		
Pd_2Au_8/HHT	B.E. (eV)	284.5	532.5	83.5	335.5	0.3	0.5
	%At.	92.3	1.4	0.2	0.1		
Au/HHT	B.E. (eV)	284.3	532.3	83.3	-	-	
	%At.	97.8	2.1	0.1			

The metals' oxidation states were studied by recording high-resolution (HR) spectra of Pd 3d and Au 4f regions (Table 3). The Pd 3d region showed two main peaks at 335.5–336.7 eV and 337.1–337.8 eV, which were assigned to Pd^0 and Pd^{II}, respectively. In addition, a satellite peak was also observed at 342.3–347.1 eV. The relative amount of Pd^0 was in the range of 62–80%, which means that most of the Pd at the surface is in its metallic form. Interestingly, a Pd^0 peak-binding energy shift of about ± 1.1 eV was observed for the bimetallic catalyst. This modification could be due to an electronic exchange from Au to Pd. Furthermore, the Au 4f region showed two peaks related to Au^0 and $Au^{\delta+}$ at about 84 eV and 85 eV, respectively. The amount of metallic Au in bimetallic catalysts was in the range of 76–51%, and the higher the amount of gold used for the synthesis, the higher the Au^0 amount.

Table 3. Results of HR spectra of Au 4f and Pd 3d regions (chemcatchem, 2021, doi.org/10.1002/cctc.202100886, in press).

		Au^0	$Au^{\delta+}$	$Au^0/Au^{\delta+}$	Pd^0	Pd^{II}	Pd_{sat}	Pd^0/Pd^{II}
Pd/HHT	B.E. (eV)	-	-	-	336.7	337.8	342.1	10.2
	%at.	-	-		80.7	7.9	11.4	
Pd_8Au_2/HHT	B.E. (eV)	84.1	85.3	1.0	335.6	337.1	347.1	3.1
	%at.	50.8	49.2		68.5	21.8	9.7	
Pd_6Au_4/HHT	B.E. (eV)	84.3	85.6	2.1	335.6	337.0	342.5	3.6
	%at.	67.8	32.2		67.1	18.8	14.1	
Pd_4Au_6/HHT	B.E. (eV)	84.1	85.6	2.1	335.5	337.2	342.3	4.8
	%at.	67.7	32.3		79.9	16.8	31.3	
Pd_2Au_8/HHT	B.E. (eV)	84.2	85.4	3.2	335.5	337.2	342.3	2.1
	%at.	76.0	24.0		61.9	29.4	8.7	
Au/HHT	B.E. (eV)	84.2	85.6	9.1	-	-	-	-
	%at.	90.1	9.9		-	-	-	

2.2. Hydrogenation Reaction

To evaluate the catalyst performance and to compare the results among all synthesized catalysts, the initial activity was evaluated using Equation (1). This parameter evaluates the catalyst conversion considering the total amount of metal used for the reaction.

Pd_8Au_2 and Pd_6Au_4 bimetallic catalysts showed an initial activity (3571 h^{-1} and 2334 h^{-1}, respectively) higher than the monometallic Pd one (2027 h^{-1}). On the contrary, the catalysts prepared with the lowest amounts of Pd (Pd_2Au_8 and monometallic Au) displayed a low activity of 214 h^{-1} and 74 h^{-1}, respectively (Figure 5). Therefore, the introduction of a second metal to Pd has a beneficial effect in terms of activity. This behavior can be explained considering that a Pd–Au alloy with a specific Pd/Au molar ratio possesses a perfect balance between the ligand effect and its lattice [31,32].

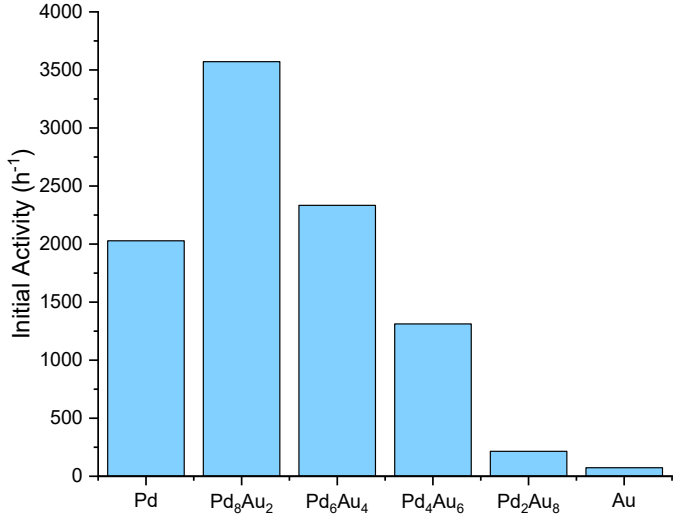

Figure 5. Initial activity of monometallic and bimetallic catalysts in the hydrogenation reaction.

Considering the conversion, all the catalysts were able to fully convert MA in 3 h, except for the Au monometallic sample, which converted about 30% of MA after 180 min. Pd, Pd_8Au_2, Pd_6Au_4, and Pd_4Au_6 catalysts showed similar conversion behavior, while Pd_2Au_4 displayed a lower conversion rate compared with the other bimetallic catalysts (Figure S1). Despite all the bimetallic catalysts reaching full conversion after 30 min (except for Pd_2Au_8), their behaviors in the first 15 min looked different. In particular, the Pd_8Au_2 catalyst gave the best performance after 15 min. Instead, monometallic Pd performance was similar to that of the Pd_6Au_4 catalyst in terms of conversion.

On the contrary, catalyst selectivity toward the intermediates and AdA strictly depended on their composition (Figure S2). The reaction first occurred with the conversion of MA to three different intermediates having different positions of the double bond. Then, the intermediates were converted to MA (Figure 6).

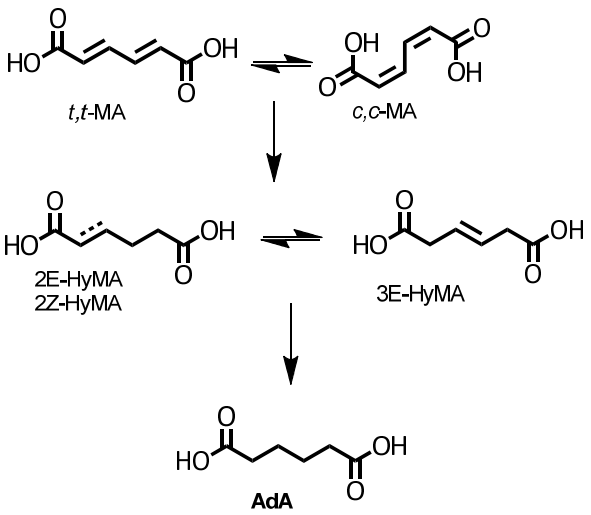

Figure 6. Scheme of MA conversion to AdA.

Considering AdA selectivity, the Pd_8Au_2 catalyst exhibited the best performance for low reaction times. Monometallic Pd, Pd_8Au_2, and Pd_6Au_4 catalysts showed 100% selectivity toward AdA after 1 h, while the Pd_4Au_6 sample was able to fully convert MA to AdA in 3 h. On the contrary, the Pd_2Au_8 catalyst showed only 60% of selectivity toward AdA after 3 h, while monometallic Au was completely inactive toward the production of bio-AdA. Interestingly, the Au monometallic catalyst showed about 70% and 25% of selectivity toward 2Z-HyMA and 2E-HyMA, respectively. Therefore, in this reaction condition, the Au/HHT catalyst could be a good candidate for the production of monounsaturated acrylic monomers.

The products' selectivity at an iso-conversion of 30% was also evaluated (Figure 7). For all the considered catalysts, the main intermediate was 2Z-HyMA. Moreover, a decreasing trend was established: the lower the Pd/Au ratio, the lower the 2Z-HyMA selectivity. On the contrary, the amount of 2E-HyMA was higher when the Pd/Au ratio decreased. Therefore, by varying the Pd/Au ratio, it is possible to synthesize a wide range of monomers by simply varying the catalyst metal composition.

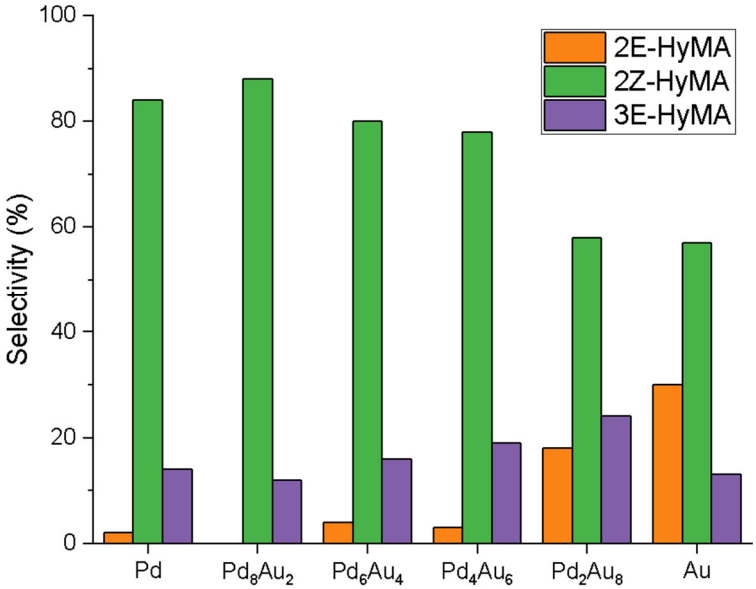

Figure 7. Intermediate selectivity after 30 min of reaction.

Considering the reaction pathway, Pd, Pd_8Au_2, and Pd_6Au_4 catalysts first converted MA to the 2Z-HyMA intermediate, which was quickly transformed to AdA. This behavior is better highlighted looking at the intermediates' concentration profiles of the Pd_4Au_2 and Pd_2Au_8 catalysts (Figure S3).

Finally, six consecutive reactions were performed by recovering the catalyst after each reaction to study catalyst recyclability. Monometallic Pd, as expected, lost its activity after the fourth recycling tests, probably due to metal leaching that occurs in an acidic environment (Figure 8). On the contrary, Pd_8Au_2 and Pd_6Au_4 catalysts maintained their activity for up to six consecutive reactions. Therefore, the bimetallic NPs are more stable against leaching, opening the possibility to be industrially attractive.

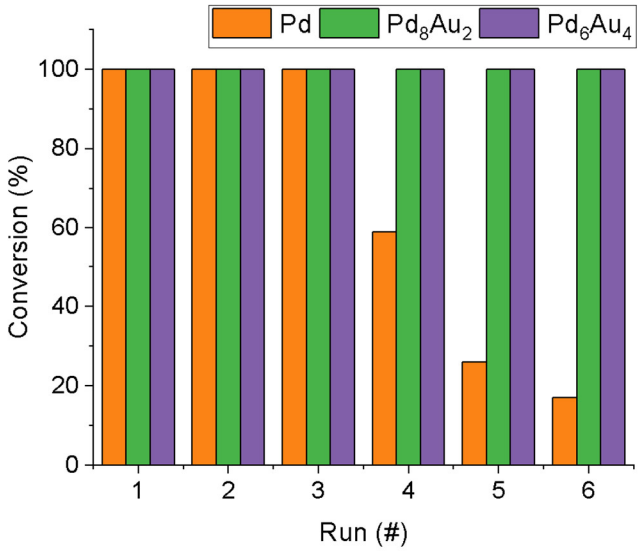

Figure 8. MA conversion after 60 min during recycling tests. #: progressive number of recycle run.

3. Experimental Section

3.1. Catalyst Synthesis

All the catalysts were synthesized using sol immobilization synthesis, as reported by Barlocco et al. [30].

Commercial HHT carbon nanofibers (CNFs) were used as a support. HHT CNFs have a surface area of about 25 m^2/g and an inner and outer diameter of 60 and 130 nm, respectively. Briefly, K_2PdCl_4 and $NaAuCl_4 \cdot 2H_2O$ were used as metal precursors, polyvinyl alcohol (PVA) as a stabilizer, and $NaBH_4$ as a reducing agent. First, the metal precursor solutions were added to 100 mL of mQ H_2O in order to reach a final total metal loading of 1% with different Au/Pd molar ratios. Then an aqueous solution of PVA (1% wt) was added with a PVA/metal weight ratio of 0.5/1. Furthermore, $NaBH_4$ was added ($NaBH_4$-to-metal molar ratio of 8/1) to reduce the metal precursor to metallic NPs. The colloidal solution was stirred for 30 min, and then 1.0 g of HHT was added to the metal NP colloid. The suspension was then acidified at pH 2 using concentrated H_2SO_4 to ensure complete deposition of NPs on the support. Finally, the obtained catalysts were filtered, washed until neutral pH, and dried at 80 °C.

3.2. Catalyst Characterization

The morphology and microstructures of the catalysts were characterized by transmission electron microscopy (TEM) using high-angle annular dark-field (HAADF) scanning transmission electron microscopy (STEM) and energy-dispersive X-ray spectroscopy (EDX). A Themis300 transmission electron microscope (Thermo Fisher Scientific), equipped with a probe aberration corrector and Super-X EDX detectors, operating at 300 kV, was used for both EDX and HAADF-STEM analyses.

X-ray photoelectron spectroscopy (XPS) analyses were performed using a Thermo Fisher Scientific K-alpha+. The samples were analyzed using a monochromatic Al X-ray source operating at 72 W. All the data were recorded at 150 eV for survey scans and at 40 eV for high-resolution (HR) spectra with a 1 eV and 0.1 eV step size, respectively. The CASAXPS (v2.3.17 PR1.1) program was used for the analysis of the XPS spectra.

3.3. Hydrogenation Reaction

The hydrogenation reactions of cis,cis-muconic acid (Sigma-Aldrich, >97%) were carried out in a batch glass reactor heated using an oil bath. The temperature was controlled by using a heating plate equipped with a thermocouple.

The reactor was filled with 25 mL of an aqueous solution of MA (0.01 M) in demineralized water and Pd–Au catalysts (1.8–3.0 mg) and then pressurized at 2 bar absolute of hydrogen. The substrate-to-metal molar ratio was 1500/1, which allowed avoiding any mass transfer limitations, as previously verified.

Batch hydrogenation reactions were conducted at 50 °C at a stirring rate of 1000 rpm, which ensured a kinetic regime. During the tests, the reaction samples were taken after 5, 15, 30, 60, 90, 120, and 180 min after quenching the reaction. The reaction products were analyzed with high-performance liquid chromatography (HPLC) equipped with an ultravisible (UV) set at 210 nm. Briefly, the reaction sample was centrifuged and then diluted using a H_2SO_4 (0.005 M) solution. The HPLC column (Rezex ROA-Organic Acid H+ (8%)) was able to separate all the intermediates, the substrate, and AdA for the evaluation of MA conversion and product selectivity. Due to the unavailability of commercial standards of the intermediates, these products were identified by ^{1}H-NMR analysis (Figures S4–S9).

Initial activity after 5 min of reaction was evaluated considering the MA reacted moles (after 5 min) and the total metal amount used for the reaction (Equation (1)).

$$Initial\ activity\ (h^{-1}) = \frac{MA\ reacted\ (mol)}{mol_{met}\ \cdot\ reaction\ time\ (h)} \quad (1)$$

3.4. Recycle Tests

Recycle tests were carried out with the same setup used for the hydrogenation reaction. The reactor was filled with 25 mL of 0.01 M MA in demineralized water and Pd–Au catalysts and then pressurized at 2 bar of hydrogen. Batch hydrogenation was conducted at 50 °C under stirring at 1000 rpm for 60 min, and then a liquid sample of the reaction mixture was analyzed with HPLC/UV to evaluate conversion. Due to the low amount of catalyst used for the reaction, it was not possible to filter and completely recover the catalyst after the reaction. Therefore, 35 mg of MA was added to the reaction mixture to restore the initial concentration of MA after each reaction. With this procedure, it was possible to evaluate MA conversion for 5 consecutive cycles.

Selectivity was not evaluated because of progressive accumulation of products in the reaction mixture.

4. Conclusions

The sol immobilization method was successfully applied for the synthesis of new bimetallic Pd–Au nanoparticles supported on high-temperature, heat-treated carbon nanofibers. The catalysts were investigated by TEM and XPS characterization. The average particle size for monometallic Pd and Au samples was 3.9 and 3.4 nm, respectively, while all the bimetallic samples showed a mean particle diameter of 3.0 nm (3.8 nm only for the Pd_4Au_6 sample). The measured loading of Pd and Au was coherent with the theoretical value for all the samples, except Pd_3Au_8 for segregated Pd nanoparticles. XPS analysis confirmed that the catalysts' surface was Pd rich and that most of the Pd at the surface was in its metallic form. Metallic Au was present, too, in the range of 76–51%.

The synthesized Pd–Au bimetallic catalysts showed higher activity than monometallic Au and Pd material in the conversion of muconic acid, dissolved in water, to adipic acid. More in detail, Pd_8Au_2 and Pd_6Au_4 bimetallic catalysts guaranteed initial activities of 3571 and 2334 h^{-1}, respectively, higher than the corresponding one obtained with monometallic Pd (2027 h^{-1}). The addition of Au to Pd allowed obtaining higher activity. Referring to our experimental conditions, bimetallic catalysts are able to promote the hydrogenation reaction with full conversion of muconic acid in 3 h. The selectivity of the process is highly dependent on the catalyst composition: the higher the amount of gold, the higher the selectivity toward the intermediates.

Recycle tests were performed to check the catalyst stability, and bimetallic samples were fully stable against the leaching phenomenon. On the contrary, the monometallic Pd sample highlighted a decrease in activity, starting from the third recycling, with a progressive decline in subsequent tests.

Supplementary Materials: The following are available online at www.mdpi.com/article/10.3390/catal11111313/s1, Figure S1. Catalyst conversion profile, Figure S2. Intermediates (A, B, and C) and AdA (D) selectivity profile using monometallic and bimetallic Pd/Au catalysts, Figure S3. Reaction profile of (A) Pd/HHT, (B) Pd8Au2/HHT, (C) Pd6Au4/HHT, (D) Pd4Au6/HHT, (E) Pd2Au8/HHT, and (F) Au/HHT catalysts. Figure S4. 1H-NMR of commercial AdA in D_2O, Figure S5. 1H-NMR of commercial t,t-MA in D_2O, Figure S6. 1H-NMR of commercial c,c-MA in D_2O, Figure S7. 1H-NMR of commercial 3E-HyMA in D_2O, Figure S8. 1H-NMR in D_2O after 60 min using Pd4Au6/HHT catalyst, Figure S9. 1H-NMR in D_2O after 120 min using Pd4Au6/HHT catalyst.

Author Contributions: Conceptualization, S.C., C.P., and A.V.; methodology, S.C., C.P., and A.V.; software, S.C.; validation, C.P. and F.M.S.; formal analysis, C.P. and A.V.; investigation, S.C., I.B., F.M.S., X.H., D.W., F.T., and A.D.M.; resources, C.P. and A.V.; data curation, S.C., I.B., F.M.S., X.H., and D.W.; writing—original draft preparation, S.C. and C.P.; writing—review and editing, all the authors; visualization, all the authors; supervision, C.P. and A.V.; project administration, C. P. and A.V.; funding acquisition, C.P. and A.V. All authors have read and agreed to the published version of the manuscript.

Funding: This research received no external funding.

Acknowledgments: This work is grateful to the Karlsruhe Nano Micro Facility (KNMF) for a long-term project for supporting the TEM work. X. Huang acknowledges the China Scholarship Council (CSC) for supporting her PhD at the Karlsruhe Institute of Technology.

Conflicts of Interest: The authors declare no conflict of interest.

References

1. Dong, H.; Zhao, J.; Chen, J.; Wu, Y.; Li, B. Recovery of Platinum Group Metals from Spent Catalysts: A Review. *Int. J. Miner. Process.* **2015**, *145*, 108–113. https://doi.org/10.1016/j.minpro.2015.06.009.
2. Liu, W.-J.; Tian, K.; He, Y.-R.; Jiang, H.; Yu, H.-Q. High-Yield Harvest of Nanofibers/Mesoporous Carbon Composite by Pyrolysis of Waste Biomass and Its Application for High Durability Electrochemical Energy Storage. *Environ. Sci. Technol.* **2014**, *48*, 13951–13959. https://doi.org/10.1021/es504184c.
3. Kaneko, A.; Ishii, Y.; Kirimura, K. High-Yield Production of *cis*,*cis*-Muconic Acid from Catechol in Aqueous Solution by Biocatalyst. *Chem. Lett.* **2011**, *40*, 381–383. https://doi.org/10.1246/cl.2011.381.
4. Yoshikawa, N.; Mizuno, S.; Ohta, K.; Suzuki, M. Microbial Production of Cis,Cis-Muconic Acid. *J. Biotechnol.* **1990**, *14*, 203–210. https://doi.org/10.1016/0168-165690009-Z.

5. Yocum, R.R.; Gong, W.; Dole, S.; Sillers, R.; Gandhi, M.; Pero, J.G. Production of Muconic Acid from Genetically Engineered Microorganisms. WO Patent 2013116244 A1, 8 August 2013.
6. Mizuno, S.; Yoshikaw, N.; Seki, M.; Mikawa, T.; Imada, Y.; Yoshikawa, N.; Seki, M.; Mikawa, T.; Imada, Y. Microbial Production of Cis,Cis-Muconic Acid from Benzoic Acid. *Appl. Microbiol. Biotecnol.* **1988**, *28*, 20–25.
7. Imada, Y.; Yoshikawa, N.; Mizuno, S.; Takashi, M. Process for Preparing Muconic Acid. U.S. Patent No. US4871667A, 1984.
8. Vardon, D.R.; Rorrer, N.A.; Salvachúa, D.; Settle, A.E.; Johnson, C.W.; Menart, M.J.; Cleveland, N.S.; Ciesielski, P.N.; Steirer, K.X.; Dorgan, J.R.; et al. Cis,Cis-Muconic Acid: Separation and Catalysis to Bio-Adipic Acid for Nylon-6,6 Polymerization. *Green Chem.* **2016**, *18*, 3397–3413. https://doi.org/10.1039/C5GC02844B.
9. Carraher, J.M.; Pfennig, T.; Rao, R.G.; Shanks, B.H.; Tessonnier, J.-P. Cis,Cis-Muconic Acid Isomerization and Catalytic Conversion to Biobased Cyclic-C_6-1,4-Diacid Monomers. *Green Chem.* **2017**, *19*, 21–25. https://doi.org/10.1039/C7GC00658F.
10. Scelfo, S.; Pirone, R.; Russo, N. Highly Efficient Catalysts for the Synthesis of Adipic Acid from Cis,Cis-Muconic Acid. *Catal. Commun.* **2016**, *84*, 98–102. https://doi.org/10.1016/j.catcom.2016.06.013.
11. Capelli, S.; Motta, D.; Evangelisti, C.; Dimitratos, N.; Prati, L.; Pirola, C.; Villa, A. Bio Adipic Acid Production from Sodium Muconate and Muconic Acid: A Comparison of Two Systems. *ChemCatChem* **2019**, *11*, 3075–3084. https://doi.org/10.1002/cctc.201900343.
12. Capelli, S.; Motta, D.; Evangelisti, C.; Dimitratos, N.; Prati, L.; Pirola, C.; Villa, A. Effect of Carbon Support, Capping Agent Amount, and Pd NPs Size for Bio-Adipic Acid Production from Muconic Acid and Sodium Muconate. *Nanomaterials* **2020**, *10*, 505. https://doi.org/10.3390/nano10030505.
13. Vardon, D.R.; Franden, M.A.; Johnson, C.W.; Karp, E.M.; Guarnieri, M.T.; Linger, J.G.; Salm, M.J.; Strathmann, T.J.; Beckham, G.T. Adipic Acid Production from Lignin. *Energy Environ. Sci.* **2015**, *8*, 617–628. https://doi.org/10.1039/C4EE03230F.
14. Roy, A.; Debnath, B.; Sahoo, R.; Chandrakumar, K.R.S.; Ray, C.; Jana, J.; Pal, T. Enhanced Catalytic Activity of Ag/Rh Bimetallic Nanomaterial: Evidence of an Ensemble Effect. *J. Phys. Chem. C* **2016**, *120*, 5457–5467. https://doi.org/10.1021/acs.jpcc.5b11018.
15. Jiang, Z.; Guo, S.; Fang, T. Enhancing the Catalytic Activity and Selectivity of PdAu/SiO2 Bimetallic Catalysts for Dodecahydro-N-Ethylcarbazole Dehydrogenation by Controlling the Particle Size and Dispersion. *ACS Appl. Energy Mater.* **2019**, *2*, 7233–7243. https://doi.org/10.1021/acsaem.9b01202.
16. Sharma, G.; Kumar, A.; Sharma, S.; Naushad, M.; Prakash Dwivedi, R.; ALOthman, Z.A.; Mola, G.T. Novel Development of Nanoparticles to Bimetallic Nanoparticles and Their Composites: A Review. *J. King Saud Univ.-Sci.* **2019**, *31*, 257–269. https://doi.org/10.1016/j.jksus.2017.06.012.
17. Jia, Q.; Segre, C.U.; Ramaker, D.; Caldwell, K.; Trahan, M.; Mukerjee, S. Structure–Property–Activity Correlations of Pt-Bimetallic Nanoparticles: A Theoretical Study. *Electrochim. Acta* **2013**, *88*, 604–613. https://doi.org/10.1016/j.electacta.2012.10.124.
18. Dellamorte, J.C.; Lauterbach, J.; Barteau, M.A. Palladium–Silver Bimetallic Catalysts with Improved Activity and Selectivity for Ethylene Epoxidation. *Appl. Catal. A Gen.* **2011**, *391*, 281–288. https://doi.org/10.1016/j.apcata.2010.06.023.
19. Barlocco, I.; Capelli, S.; Zanella, E.; Chen, X.; Delgado, J.J.; Roldan, A.; Dimitratos, N.; Villa, A. Synthesis of Palladium-Rhodium Bimetallic Nanoparticles for Formic Acid Dehydrogenation. *J. Energy Chem.* **2021**, *52*, 301–309. https://doi.org/10.1016/j.jechem.2020.04.031.
20. Patankar, S.C.; Sharma, A.G.; Yadav, G.D. Biobased Process Intensification in Selective Synthesis of γ-Butyrolactone from Succinic Acid via Synergistic Palladium–Copper Bimetallic Catalyst Supported on Alumina Xerogel. *Clean Technol. Environ. Policy* **2018**, *20*, 683–693. https://doi.org/10.1007/s10098-017-1381-6.
21. Jin, X.; Zhao, M.; Vora, M.; Shen, J.; Zeng, C.; Yan, W.; Thapa, P.S.; Subramaniam, B.; Chaudhari, R.V. Synergistic Effects of Bimetallic PtPd/TiO2 Nanocatalysts in Oxidation of Glucose to Glucaric Acid: Structure Dependent Activity and Selectivity. *Ind. Eng. Chem. Res.* **2016**, *55*, 2932–2945. https://doi.org/10.1021/acs.iecr.5b04841.
22. Riahi, G.; Guillemot, D.; Polisset-Thfoin, M.; Khodadadi, A.A.; Fraissard, J. Preparation, Characterization and Catalytic Activity of Gold-Based Nanoparticles on HY Zeolites. *Catal. Today* **2002**, *72*, 115–121. https://doi.org/10.1016/S0920-586100485-0.
23. Scott, R.W.J.; Wilson, O.M.; Oh, S.-K.; Kenik, E.A.; Crooks, R.M. Bimetallic Palladium−Gold Dendrimer-Encapsulated Catalysts. *J. Am. Chem. Soc.* **2004**, *126*, 15583–15591. https://doi.org/10.1021/ja0475860.
24. Schwartz, T.J.; Lyman, S.D.; Motagamwala, A.H.; Mellmer, M.A.; Dumesic, J.A. Selective Hydrogenation of Unsaturated Carbon–Carbon Bonds in Aromatic-Containing Platform Molecules. *ACS Catal.* **2016**, *6*, 2047–2054. https://doi.org/10.1021/acscatal.6b00072.
25. Ma, C.; Du, Y.; Feng, J.; Cao, X.; Yang, J.; Li, D. Fabrication of Supported PdAu Nanoflower Catalyst for Partial Hydrogenation of Acetylene. *J. Catal.* **2014**, *317*, 263–271. https://doi.org/10.1016/j.jcat.2014.06.018.
26. Yang, X.; Chen, D.; Liao, S.; Song, H.; Li, Y.; Fu, Z.; Su, Y. High-Performance Pd–Au Bimetallic Catalyst with Mesoporous Silica Nanoparticles as Support and Its Catalysis of Cinnamaldehyde Hydrogenation. *J. Catal.* **2012**, *291*, 36–43. https://doi.org/10.1016/j.jcat.2012.04.003.
27. Luo, L.; Duan, Z.; Li, H.; Kim, J.; Henkelman, G.; Crooks, R.M. Tunability of the Adsorbate Binding on Bimetallic Alloy Nanoparticles for the Optimization of Catalytic Hydrogenation. *J. Am. Chem. Soc.* **2017**, *139*, 5538–5546. https://doi.org/10.1021/jacs.7b01653.
28. Crespo-Quesada, M.; Dykeman, R.R.; Laurenczy, G.; Dyson, P.J.; Kiwi-Minsker, L. Supported Nitrogen-Modified Pd Nanoparticles for the Selective Hydrogenation of 1-Hexyne. *J. Catal.* **2011**, *279*, 66–74. https://doi.org/10.1016/j.jcat.2011.01.003.

29. Turáková, M.; Králik, M.; Lehocký, P.; Pikna, Ľ.; Smrčová, M.; Remeteiová, D.; Hudák, A. Influence of Preparation Method and Palladium Content on Pd/C Catalysts Activity in the Liquid Phase Hydrogenation of Nitrobenzene to Aniline. *Appl. Catal. A Gen.* **2014**, *476*, 103–112. https://doi.org/10.1016/j.apcata.2014.02.025.
30. Barlocco, I.; Capelli, S.; Lu, X.; Bellomi, S.; Huang, X.; Wang, D.; Prati, L.; Dimitratos, N.; Roldan, A.; Villa, A. Disclosing the Role of Gold on Palladium—Gold Alloyed Supported Catalysts in Formic Acid Decomposition. *ChemCatChem* **2021**, *13*, 4210–4222. https://doi.org/10.1002/cctc.202100886.
31. Xing, Z.; Guo, Z.; Chen, X.; Zhang, P.; Yang, W. Optimizing the Activity of Pd Based Catalysts towards Room-Temperature Formic Acid Decomposition by Au Alloying. *Catal. Sci. Technol.* **2019**, *9*, 588–592. https://doi.org/10.1039/C8CY02402B.
32. Wang, Q.; Chen, L.; Liu, Z.; Tsumori, N.; Kitta, M.; Xu, Q. Phosphate-Mediated Immobilization of High-Performance AuPd Nanoparticles for Dehydrogenation of Formic Acid at Room Temperature. *Adv. Funct. Mater.* **2019**, *29*, 1903341. https://doi.org/10.1002/adfm.201903341.